
Proceedings Paper:
Beattie, N.S., See, P., Zoppi, G. et al. (6 more authors) (2018) Design and fabrication of InAs/GaAs QD based intermediate band solar cells by quantum engineering. In: 2018 IEEE 7th World Conference on Photovoltaic Energy Conversion (WCPEC) (A Joint Conference of 45th IEEE PVSC, 28th PVSEC & 34th EU PVSEC). 2018 IEEE 7th World Conference on Photovoltaic Energy Conversion (WCPEC) (A Joint Conference of 45th IEEE PVSC, 28th PVSEC & 34th EU PVSEC), 10-15 Jun 2018, Waikoloa Village, HI, USA. IEEE , pp. 2747-2751. ISBN 9781538685303

https://doi.org/10.1109/pvsc.2018.8547630

Design and fabrication of InAs/GaAs QD based intermediate band solar cells by quantum engineering

N. S. Beattie[(a)], P. See[(b)], G. Zoppi[(a)], P. M. Ushasree[(a)], M. Duchamp[(c)], I. Farrer[(d)], V. Donchev[(e)], D. A. Ritchie[(f)], and S. Tomić[(g)]

[(a)]Northumbria University, Newcastle upon Tyne, NE1 8ST, UK, [(b)]National Physical Laboratory, Teddington, TW11 0LW, UK, [(c)]Nanyang Technical University, Singapore 639798, Singapore, [(d)]University of Sheffield, Sheffield, S1 3JD, UK, [(e)]Sofia University "St. Kliment Ohridski", BG-1164 Sofia, Bulgaria, [(f)]University of Cambridge, Cambridge, CB3 0HE, UK, [(g)]University of Salford, Manchester M5 4WT, UK

***Abstract*—The efficiency of a solar cell can be substantially increased by opening new energy gaps within the semiconductor band gap. This creates additional optical absorption pathways which can be fully exploited under concentrated sunlight. Here we report a new approach to opening a sizeable energy gap in a single junction GaAs solar cell using an array of small InAs QDs that leads directly to high device open circuit voltage. High resolution imaging of individual QDs provides experimentally obtained dimensions to a quantum mechanical model which can be used to design an optimised QD array. This is then implemented by precisely engineering the shape and size of the QDs resulting in a total area (active area) efficiency of 18.3% (19.7%) at 5 suns concentration. The work demonstrates that only the inclusion of an appropriately designed QD array in a solar cell has the potential to result in ultra-high efficiency under concentration.**

***Index Terms*—Intermediate Band Solar Cell, QDs, Photovoltaics, High Efficiency**

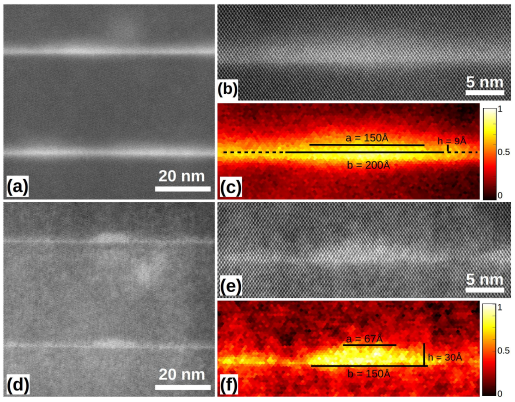

Fig. 1. (a, b, d, e) HAADF-STEM images and (c, f) local mean intensity maps of individual QDs b and f respectively. (a-c) QD-IBSCs without and (d-f) with quantum engineering.

I. Introduction

For the IBSC to function correctly, the semiconductor valence band (VB), intermediate band (IB) and conduction band (CB) must all be electronically isolated. This requires well-separated quasi-Fermi levels under external illumination and pure zero density of states (DOS) between the IB and CB [1]. Under ideal conditions, IBSC theory predicts a maximum efficiency of 63% for an energy separation $E_{VB,IB} = 1.2$ eV between the VB and the IB, and $E_{IB,CB} = 0.7$ eV between the IB and the CB [2]. The most studied experimental IBSC prototype is based on incorporating an array of self-assembled InAs semiconductor QDs within the intrinsic region of a GaAs *pin* diode. This gives rise to the QD intermediate band solar cell (QD-IBSC). Although $E_{IB,CB}$ is less than ideal ($\sim 5-120$ meV) for this material system, a realistically achievable solar energy conversion of 34% under concentration is nevertheless predicted [3] and it is notable that the first demonstration of a photovoltaic concentrator module using QD-IBSCs was recently reported [5].

In this work we present a new experimental approach to opening a clear energy gap between an IB of quantum states and the CB in a QD-IBSC. By precisely controlling the shape and size of the QDs in the QD array used to create the IB we can, for the first time in an IBSC implement a quantum mechanical design which simultaneously fulfils the objectives of IB regime operation and high device open circuit voltage (V_{oc}) without the need for additional wider band gap barrier layers. The findings provide a pathway to high efficiency InAs QD-IBSCs and an approach to creating ultra-high efficiency III-V multijunction solar cells by virtue of the compatibility of the technologies [6].

II. Results and Discussions

Solar cell device wafers were grown *via* MBE and included 20 stacked layers of InAs self-assembled QDs in the intrinsic region of a GaAs *pin* diode. Here, we capitalise on the quality and precision of MBE growth to create QD arrays that do not require strain compensation [7]. Furthermore, transferring a technique from light emitting applications [8] affords control over the shape and size of the QDs at the nanometre scale [9]. It therefore offers a way to engineer the discrete energy levels within the QDs and ultimately the separation between the IB and the CB. We refer to this growth technique as *quantum engineering*. Controlling the temperature profile and the spacer layer depth (near atomic precision) at which such quantum engineering is applied, allows the fabrication of highly uniform QD arrays too.

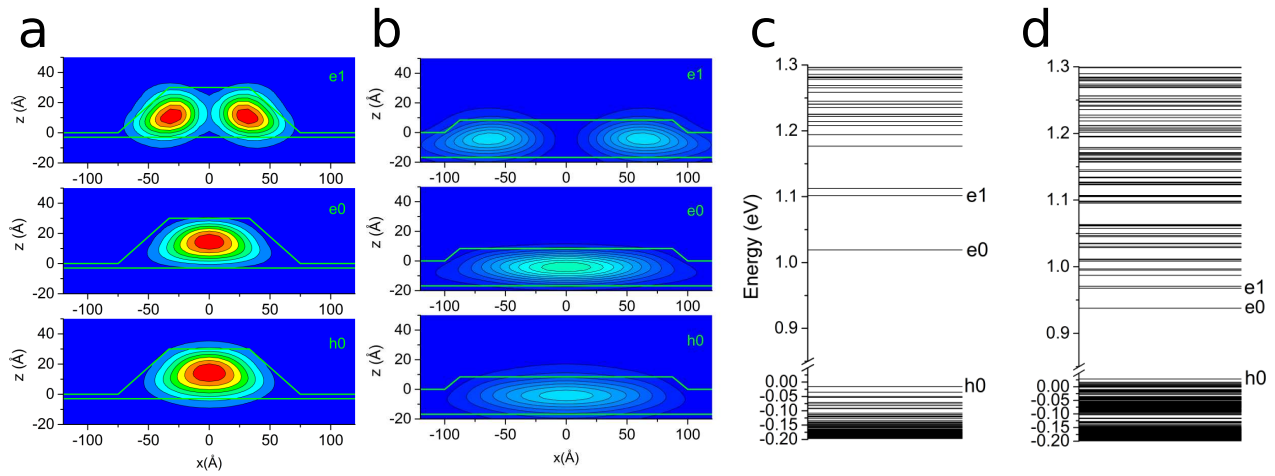

Fig. 2. (a, b) Charge densities and (c, d) electronic structure for individual quantum dots calculated using dimensions obtained from STEM measurements. (a, c) correspond to a quantum dot from a quantum engineered array while (b, d) correspond to a reference array. e_0 and e_1 denote ground and first excited states in the CB and h_0 is the ground state in the VB.

In Fig. 1 we present the high resolution high-angle annular-dark-field (HAADF) scanning transmission electron microscopy (STEM) images of individual QDs from a reference QD-IBSC, (a)-(c), and a quantum engineered QD-IBSC,(d)-(f). The imaging conditions were chosen to acquire HAADF-STEM images which are approximately proportional to the square of the atomic number. Further, the white contrast indicates the presence of a large indium concentration compared to the surrounding GaAs matrix. The projected dimensions of the QDs are extracted from the local mean intensity maps which are bounded by a truncated pyramid shape with QD base length b, length at the site of truncation a and height h. Note that the hight of the QDs, h, has been estimated from the top of the wetting layer and the top of the QD in figures 1 (c) and between the bottom and the top of the QD in figure 1(f) due to almost negligible WL. Such estimated QDs dimensions have been passed to the simulations. From these data the extracted dimensions are, $a = 150$ Å, $b = 200$ Å and $h = 9$ Å, and $a = 67$ Å, $b = 150$ Å and $h = 30$ Å, for the reference and quantum engineered QD-IBSC respectively. Using the QD shape and size dimensions obtained from the STEM, we modelled the QD arrays in the reference QD-IBSC and the quantum engineered QD-IBSC using a $\mathbf{k}\cdot\mathbf{p}$ method combined with periodic boundary conditions in the vertical direction as described in greater detail elsewhere [1], [3], [4]. Using the quantum dot shape and size dimensions obtained from the STEM data, we modelled the quantum dot arrays in the reference QD-IBSC and the quantum engineered QD-IBSC using a combination of a $\mathbf{k}\cdot\mathbf{p}$ method combined with periodic boundary conditions in the vertical direction and described in greater detail elsewhere [4], [1], [3]. In Figure 2(a) and (b) we plot the contours of the charge densities of the electron ground state (e0), first excited state (e1) and the hole ground state (h0) for the two quantum dot arrays. Here e0, e1 and h0 correspond to the IB, CB and VB respectively. It is evident that the quantum engineered QD-IBSC (Figure 2(a)) results in significant localisation of e0, e1, and h0 in the quantum dot, while for the reference QD-IBSC (Figure 2(b)), a significant part of the charge density is actually localised in the wetting layer. In this case the whole layer behaves more like a quantum well with modulated z dimension.

Figure 2(c) and (d) show the single particle energy spectra for the two structures. The quantum engineered QD-IBSC exhibits a clear energy separation between e0 and e1 states of $\Delta E_{\mathrm{e0,e1}} = 83$ meV which is more than twice that of the reference QD-IBSC where $\Delta E_{\mathrm{e0,e1}} = 30$ meV, and also more than three times the thermal energy ($k_B T = 26$ meV) at room temperature. This is clear indication that the quantum engineered QD-IBSC will provide much better conditions for the formation of the quasi-Fermi level separation between the IB and CB under external illumination.

In order to clearly identify the contribution of the IB to the optical properties of the two quantum dot arrays in the quantum engineered QD-IBSC and the reference QD-IBSC, we calculate their absorption spectra within the dipole approximation as: [1], [3]

$$\begin{aligned} \alpha(\hbar\omega) &= \frac{\pi e^2}{c\epsilon_0 m_0^2 \bar{n}\omega\Omega} \\ &\times \sum_{\mathbf{K}}\sum_{i,f} |\langle i|\hat{\mathbf{e}}\cdot\ \mathbf{p}(\mathbf{K})|f\rangle|^2 \\ &\times \delta[E_f(\mathbf{K}) - E_i(\mathbf{K}) - \hbar\omega](f_i - f_f), \end{aligned} \tag{1}$$

where e is the electron charge, $\bar{n}$ the refractive index, ϵ_0 the dielectric permittivity of vacuum, c the speed of light, Ω the volume of the structure, $\hat{\mathbf{e}}$ the unit vector of light polarization, and $\mathbf{p}(\mathbf{K})$ is the momentum operator. The optical dipole matrix element is given by $\langle i|\hat{\mathbf{e}}\cdot\ \mathbf{p}(\mathbf{K})|f\rangle$, and varies inside the 1D Brillouin zone (BZ) of an QD array. The initial and final state energies are $E_i(\mathbf{K})$ and $E_f(\mathbf{K})$, which also varies throughout

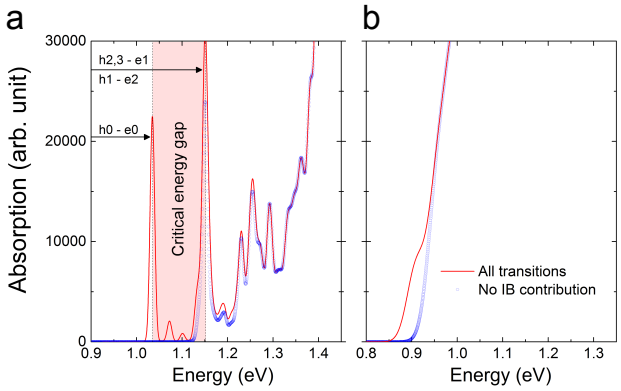

Fig. 3. Absorption spectra of QD arrays corresponding to (a) a quantum engineered QD-IBSC and (b) a reference QD-IBSC.

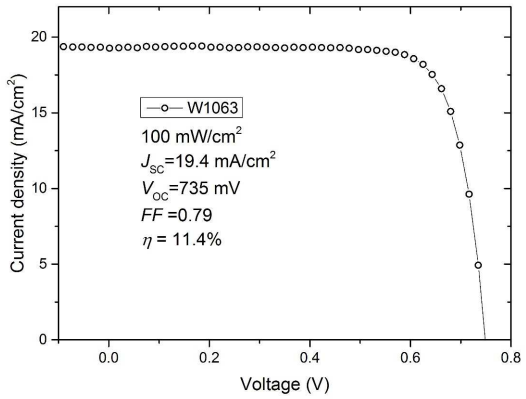

Fig. 4. JV characteristic of unroped InAs/GaAs QD array with largely inhomogeneous QDs, and with the $V_{\rm oc} = 735$ mV.

the QD array BZ, $\hbar\omega$ is the photon energy, and $f_{i(f)}$ is the initial (final) state Fermi-Dirac distribution function.

Our calculations reveal that for the the quantum engineered QD-IBSC (Fig. 1(f)) significant localisation of e0, e1, and h0 inside the QD region, while for the reference QD-IBSC (Fig. 1(c)), a significant part of the charge density is actually localised in the wetting layer. In this case the whole layer behaves more like a quantum well with modulated z dimension.

Figure 3 shows two absorption spectra for each array: one between all VB and CB states (solid line) and one between all VB and CB states except those originating from e_0 (open circles). It is evident that for the quantum engineered QD-IBSC (Figure 3(a)) clear regions of zero DOS exists between e1 and e0. This is the signature of an energetically isolated IB.

In our experimental approach, we use first our test device sample, W1063, to perform the surface photo-voltage measurement in order to identify the position of the energy levels in QD array. The sample was with unroped InAs/GaAs QDs of surface density $\sim 4 \times 10^{10}$ cm^{-2}. This density was obtained from the TEM data. Increasing this density would increase the photocurrent via a greater number of IB states. From the analysis of TEM data, we have identified that W1063 is free from strain-related defects such as threading dislocations, hence we concluded of high quality.

Figure 4 shows the JV characteristic obtained under 1-sun irrandiance. Since the W1063 does not contain an anti-reflective coating, the direct comparison with our final device is not possible in terms of the short circuit current density ($J_{\rm sc}$) which is considerably lower in W1063. However, the direct comparison between the open circuit voltages ($V_{\rm oc}$) would be viable. Compared W1063 with the quantum engineered QD-IBSC the $V_{\rm oc}$ is smaller for $\sim$100 mV in W1063, which we attribute to the inhomogeneous QD size distribution. This drop in $V_{\rm oc}$ is explained with the results obtained from the surface photo voltage measurements, Figure 5. From Figure 5 we have identified of the average ground (IB) and first excited (CB) states QD array states at 1.075 eV and 1.134 eV respectively.

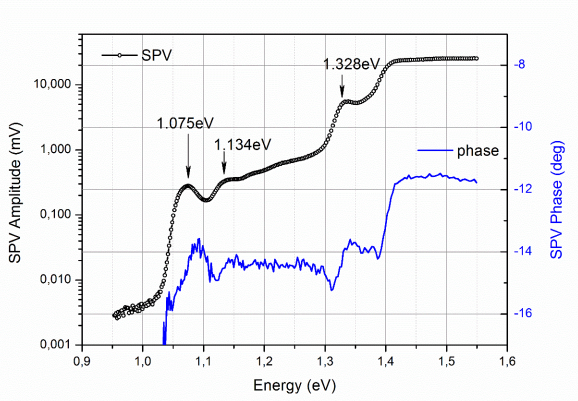

Fig. 5. The surface photo voltage measurements of W1063 with $\Delta E_{e0,e1} = 59$ meV. The arrow at 1.328 eV indicates the wetting layer states, while the plateau at 1.42 eV and above is associated to the GaAs matrix.

This corresponds to an energetic splitting of $\Delta E_{e0,e1} = 59$ meV i.e. considerably less than once achieved in the optimised a quantum engineered QD-IBSC, discussed below.

Furthermore, since smaller QDs [4] are preferable to maximise the energetic separation between IB and CB, the experimental guidance would therefore be to to lower the MBE growth temperature of the QD layer with the objective of achieving greater coverage (increased density) of smaller quantum dots.

The W1063 and the reference QD-IBSC (Fig. 3(b)) strong hybridisation exists between all states in the CB and there is no clear opening of a second energy gap associated with an IB. Due to such strong hybridisation of the states, the effect of the QD array appears only as a slight shoulder in the data which pushes the absorption edge to lower energy. This behaviour has been been experimentally observed by several groups, (see Review [10]), but unfortunately the resulting increase in J_{sc} comes at the expense of significant reduction in V_{oc} due to the loss of IB features, i.e. lost of the quasi–Fermi levels separation between IB and CB under illumination. This has been a key bottleneck in the development of the QD-IBSC

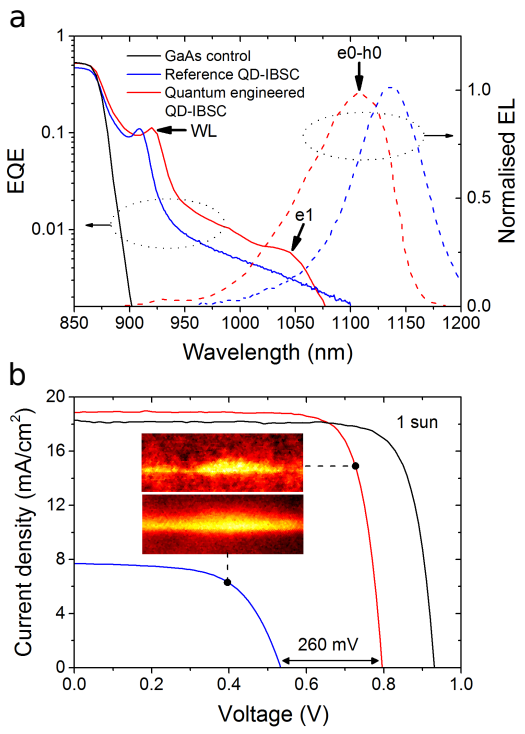

Fig. 6. (a) EQE (solid), normalized EL spectra (dashed) and (b) JV curves for a GaAs control solar cell, a reference QD-IBSC and a quantum engineered QD-IBSC. The inset to (b) shows representative quantum engineered (upper) and reference (lower) QDs in each device. Note that the same legend applies to (a) and (b).

technology and our work demonstrates that the advantages of the IBSC are indeed accessible in this system if the QD array is appropriately designed.

Figure 6(a) shows the external quantum efficiency (EQE) for a GaAs control solar cell, a reference QD-IBSC and a quantum engineered QD-IBSC. The reference QD-IBSC and the quantum engineered QD-IBSC are constructed from arrays of the QDs shown in Figs 1(c) and (f) respectively. A larger range of EQE for these SCs is presented elsewhere [11] and here we focus on the region beyond the GaAs band edge. As expected, the EQE signal for the GaAs control SC falls sharply at the GaAs band edge, while the EQE for the QD-IBSCs extends to longer wavelengths. This behaviour is attributed to VB to IB optical transitions. The important point here however, is the difference between the EQE for the quantum engineered QD-IBSC compared with the reference QD-IBSC. While both SCs exhibit a InAs wetting layer characteristic around 1.35 eV, only the quantum engineered QD-IBSC presents a shoulder at approximately 1.19 eV. From room temperature electroluminescence (EL) measurements, Fig.6(a), we determined this to be the first excited state e1. The contribution of the ground states in the EQE is beyond the range of the detector. The difference between e1 and the ground state transition e0−h0 determined from EL is 70 meV is in good agreement with our theory.

Figure 6(b) shows that quantum engineered QD-IBSC has

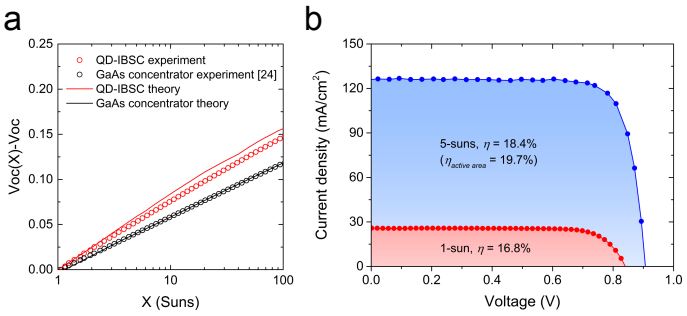

Fig. 7. (a) Variation of the open circuit voltage offset, $V_{\rm oc}(X)-V_{\rm oc}(X=1)$ as a function of the light concentration X, for a quantum engineered QD-IBSC and a single gap conventional GaAs solar cell. Open symbols represent experiment and solid lines theory. (b) JV characteristic for an optimised quantum engineered QD-IBSC at 1-sun and 5-suns irradiance.

increased V_{oc} by a remarkable 260 mV relative to the reference QD-IBSC. In summary, changing the shape and size of the QDs significantly affects the macroscopic performance of a QD-IBSC and in distinct contrast to other work, no strain balancing layers or high energy barriers were required to achieve this result.

The observed increase in $V_{\rm oc}$ caused by quantum engineering the InAs QD array at the nanometre scale follows directly from the creation of an IB band that is separated by a region of zero DOS from the CB [12]. To further examine the influence of such a band on the device performance, we measured the evolution of V_{oc} for a quantum engineered QD-IBSC as a function of optical concentration (X suns) up to $X = 100$ using a flash lamp solar simulator. Fig. 7(a) shows the difference between the open circuit voltage as a function of concentration $V_{oc}(X)$ and V_{oc} $(X = 1)$ for a quantum engineered QD-IBSC and a high performance single energy gap GaAs concentrator solar cell . It is clear from figure 7(a) that this difference increases at a faster rate (super-linearly on a logarithmic scale) for the quantum engineered QD-IBSC than for the high performance GaAs solar cell. Such super-linear behaviour is the signature of three or more energy gaps in the device. On the other hand for a conventional single gap SC $V_{oc} \propto (kT/q)\ln X$ i.e. linearly on a log scale. In addition to the experimental data in figure 7(a), we have found that the evolution of V_{oc} for both the quantum engineered QD-IBSC and the GaAs concentrator are in good agreement with theory. As can be seen in Fig.7(b), application of our quantum engineering technique increased the 1-sun V_{oc} to 840 mV. Furthermore, the addition of a dual layer ZnS/MgF_2 anti-reflection coating on the surface and a back surface AlGaAs reflector resulted in $J_{sc} = 26$ mA/cm^2. The 1-sun JV characteristic shown in figure 7(b) is taken from one of five devices from the same device processing batch. The high uniformity of our devices is demonstrated by average values of $V_{oc} = 822 \pm 14$ mV, $J_{sc} = 25.9 \pm 0.2$ mA/cm^2, fill factor $FF = 76.3 \pm 1.2$, efficiency $\eta = 16.3 \pm 0.5\%$. The equivalent parameter set for seven GaAs control SCs from the same processing batch is: $V_{oc} = 891 \pm 60$ mV,

$J_{sc} = 25.0 \pm 1.27$ mA/cm^2, fill factor $FF = 75.3 \pm 2.0$, efficiency $\eta = 16.7 \pm 1.2\%$.

The real power of the IBSC becomes clear under concentrated sunlight where not only does V_{oc} increase at a superior rate to a single energy gap device, Fig7(a), but so also does J_{sc}. This is because the additional photocurrent resulting from the IB [13] has a quadratic dependence on the incident power [14]. We have previously reported $V_{oc} = 985$ mV at 500-suns obtained using suns-V_{oc} measurements. Figure 7(b) shows the JV curve for a quantum engineered QD-IBSC at 5-suns obtained using a flash-lamp simulator which was cross-calibrated with the 1-sun solar simulator for accuracy. The results show excellent performance up to 5-suns concentration with little degradation of the fill factor and analysis of the evolution of V_{oc} with concentration indicates the diode ideality factor to be $n = 1.2$. This is further evidence of the material quality as it approaches the ideal value of $n = 1$ for any optoelectronic *pn*-junction device. The efficiency of the device shown in Fig7(b) is $\eta = 18.4\%$ which increases to a record efficiency under concentration of 19.7% when the area of the contacts is taken into account (the active area efficiency). [15] To the best of our knowledge this is the highest reported efficiency for a InAs QD-IBSC.

ACKNOWLEDGMENTS

The authors are grateful to Alex Savidis and Solar Capture Technologies Ltd. for providing access to the flash lamp solar simulator used in the concentration measurements. S.T. wishes to thank the Royal Society, London for the supporter under RG120558. V.D. wishes to thank Bulgarian National Science Fund (contract DKOST 01/16). N.B., V.D., and S.T, wishes to thank the EU COST Action MP1406 for their contribution. The authors also acknowledge financial support from the European Union under the Seventh Framework Programme, reference 312483-ESTEEM2.

REFERENCES

[1] Tomić, S. Intermediate-band solar cells: Influence of band formation on dynamical processes in InAs/GaAs QD arrays. *Phys. Rev. B* **2010**, *82*, 195321

[2] Luque, A.; Martí, A. Increasing the efficiency of ideal solar cells by photon induced transitions at intermediate levels. *Phys. Rev. Lett.* **1997**, *78*, 5014–5017

[3] Tomić, S.; Sogabe, T.; Okada, Y. In-plane coupling effect on absorption coefficients of InAs/GaAs QD arrays for intermediate band solar cell. *Prog. Photovolt.: Res. Appl.* **2014**, *23*, 546–558

[4] Tomić, S.; Jones, T.S.; Harrison, N.M. Absorption characteristics of a quantum dot array. *Appl. Phys. Lett.* **2008**, *93*, 263105

[5] Sogabe, T.; et al. Intermediate-band dynamics of quantum dots solar cell in concentrator photovoltaic modules. *Sci. Rep.* **2014**, *4*, 4792

[6] Kerestes, C. et al. Fabrication and analysis of multijunction solar cells with a QD (In)GaAs junction. *Prog. Photovolt.: Res. Appl.* **2013**, *22*, 1172–1179

[7] Nuntawong, N.; Tatebayashi, J.; Wong, P. S.; Huffaker, D. L. Localized strain reduction in strain-compensated InAs/GaAs stacked QD structures. *Appl. Phys. Lett.* **2007**, *90*, 163121

[8] Haffouz, S. et al. Growth and fabrication of quantum dots superluminescent diodes using the indium-flush technique: A new approach to controlling the bandwidth. *J. Crystal Growth* **2009**, *311*, 1803–1806

[9] Keizer, J. G. et al., An atomically resolved study of InGaAs QD layers grown with an indium flush step. *Nanotechnology* **2010**, *21*, 215705

[10] Luque, A.; Martí, A.; Stanley, C. Understanding intermediate band solar cells. *Nat. Photon.* **2012**, *6*, 146–152

[11] Beattie, N. S. et al. Analysis of InAs/GaAs QD solar cells using suns-Voc measurements. *Sol. Energy Mater. Sol. Cells* **2014**, *130*, 241–245

[12] Bailey, C. G. et al., Near 1V open circuit voltage InAs/GaAs QD solar cells. *Appl. Phys. Lett.* **2011**, *98*, 163105

[13] Datas, A. et al., Intermediate band solar cell with extreme broadband spectrum quantum efficiency. *Phys. Rev. Lett.* **2015**, *114*, 157701

[14] Li, T.; Dagenais, M. Non-reasonant below-bandgap two-photon absorption in QD solar cells. *Appl. Phys. Lett.* **2015**, *106*, 171101

[15] Beattie, N. S. et al., Quantum engineering of InAs/GaAs quantum dot based intermediate band solar cells. *ACS Photonics* **2017**, *4*, 2745–2750